

# Surface-Cross-linked Protein-like Single-Chain Nanoparticle Globules Unexpectedly Stabilized with a Low Cross-linking Degree

Lei Zhang, Xu-Ze Zhang, Jia-Tong Lyu, Lin-Xiuzi Yu, Chun-Yu Wang, Zhao-Yan Sun, Zhong-Yuan Lu, and Hu-Jun Qian\*



Cite This: *Macromolecules* 2024, 57, 858–868



Read Online

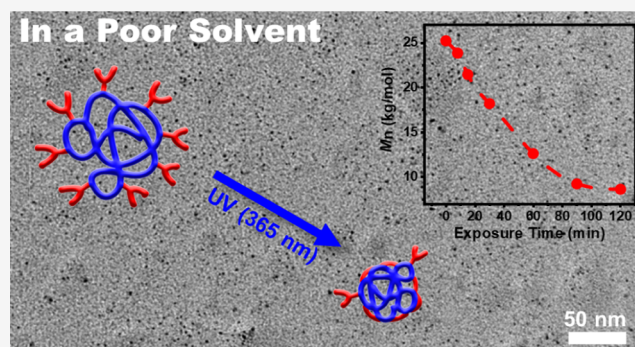
ACCESS |

Metrics & More

Article Recommendations

Supporting Information

**ABSTRACT:** Single-chain nanoparticles (SCNPs) are an emerging new nanomaterial with promising potential for exhibiting compactly collapsed globular nanostructures and associated functions, like proteins. However, the state-of-the-art synthesis approaches often result in SCNPs with diverse morphologies and loosely packed characteristics, even with an ample presence of cross-linkers, resembling sparse structures found in intrinsically disordered proteins. Herein, we present a facile strategy to fabricate protein-like compact SCNP globules using a low content of solvophilic photoreactive agents in a single-component poor solvent via flow photochemistry. Photoreactive agents in our system serve a dual purpose: acting as stabilizing agents that decorate the surface of the precollapsed precursor globules in the poor solvent and cross-linking with neighboring segments in situ upon UV irradiation on the globule surfaces. These cross-linked globules become effectively locked and remain stable when transferred into a good solvent. Computer simulations demonstrate that surface cross-linking reactions primarily occur between cross-linkers and neighboring monomers positioned at long contour distances along the chain backbone. This mechanism locks up the precollapsed protein-like SCNP globules with high efficiency; an extremely low cross-linker content of 1.6 mol % can result in an obvious reduction in molecular size. Small-angle X-ray scattering (SAXS) measurements also confirm the formation of compactly collapsed globule structures. Moreover, by varying the UV irradiation time, the degree of collapse in the SCNPs can be precisely controlled. The residual cross-linkers on the surface render the formed SCNPs reactive, thus allowing for further polymerization into hierarchical multifunctional self-assembly structures.



## INTRODUCTION

Inspired by the intricate three-dimensional (3D) folding observed in natural proteins,<sup>1</sup> single-chain nanoparticles (SCNPs) have emerged as a prominent focus in chemistry and nanoscience.<sup>2–11</sup> These SCNPs are nanostructures formed through the intramolecular cross-linking or collapsing of individual polymer chains. As a new type of soft nanomaterial, SCNPs exhibit diverse characteristics that make them suitable for various fields, such as in catalysis,<sup>12–17</sup> biomedical applications,<sup>18–21</sup> and optical materials.<sup>22–25</sup> Beyond their diverse applications, an ultimate goal is to mimic the folding patterns found in biomacromolecules, such as proteins, into well-defined 3D-folded structures to understand their associated functions. However, the efficient fabrication of such protein-like globular structures remains a major challenge.

It is well-known that proteins have a funnel-shaped energy landscape with few low-energy, native globule conformations at the bottom while many more unfolded open structures along the downhill pathway.<sup>1</sup> Hydrogen bonding between amino acids was considered as a primary endogenic physical code for protein folding. In this context, many efforts have been

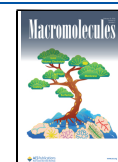
devoted to synthesizing SCNPs with various cross-linking chemistry.<sup>26–34</sup> However, after conducting an extensive survey of the literature in this direction, Pomposo et al.<sup>35</sup> found that most synthetic SCNPs exhibited noncompact and nonglobular morphologies resembling intrinsically disordered proteins (IDPs) with locally compact regions connected by flexible linkers.<sup>36</sup> Recent simulations<sup>29,37,38</sup> have shed light on the formation of IDP-like noncompact structures, attributing them to a combinational effect of the self-avoiding chain conformations and the intrachain cross-linking reaction pathway. To avoid undesired interchain cross-linking, SCNPs are often fabricated under ultradilute good solvent conditions.<sup>26,39,40</sup> This ensures that precursor chains are sufficiently separated from each other, existing in a fully

**Received:** September 13, 2023

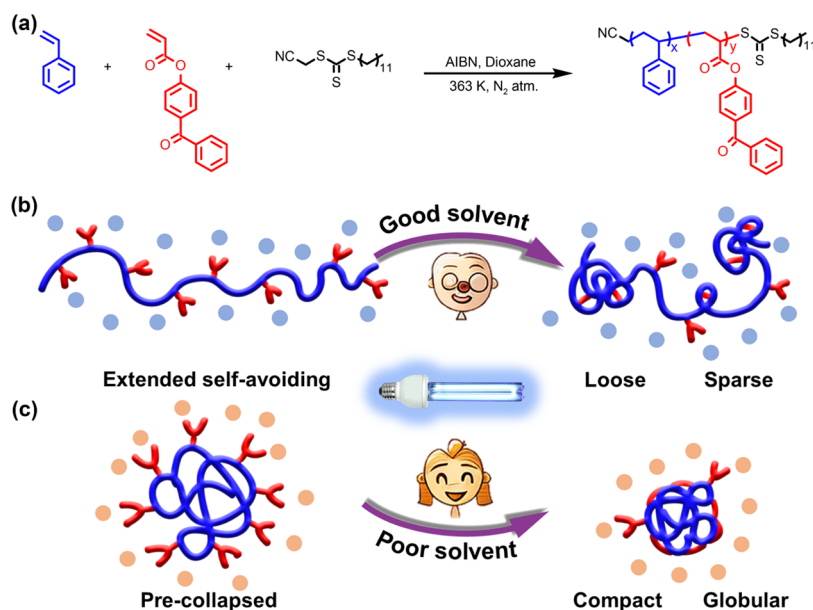
**Revised:** January 2, 2024

**Accepted:** January 3, 2024

**Published:** January 13, 2024



**Scheme 1.** (a) Synthesis of PS-ABP Precursors through RAFT Random Copolymerization and the Cross-Linking Process of PS-ABP in Different Solvents: (b) A Good Solvent and (c) A Poor Solvent



solvated state with extended self-avoiding chain conformations. Under such conditions, local intrachain cross-linking reactions occur more readily between monomer pairs with short-contour distances along the chain backbone and physically close proximity in space, consequently forming IDP-like structures with locally compact domains connected via flexible chain segments. Similarly, Zimmerman<sup>41</sup> examined the ring-closing metathesis (RCM)-mediated cross-linking of dendrimers and their subunits and demonstrated that geometrical preferences may be used to control the location of cross-linking within a macromolecular architecture.

On the other hand, it is well-established that the ordered folding and 3D structure of protein originate from a delicate balance of noncovalent interactions, such as hydrophobic/hydrophilic and polar/nonpolar interaction pairs.<sup>42–45</sup> To mimic this intricate interplay of interactions during the synthesis of SCNPs, ter Huurne, Palmans, and Meijer<sup>46–48</sup> demonstrated that the delicate balance between intra- and intermolecular self-assembly can be effectively regulated by tuning the hydrophilic/hydrophobic interactions of the polymers using a supramolecular approach. By following an appropriate collapse pathway, compact and stable SCNPs can be formed.<sup>49,50</sup> Additionally, Gormley and co-workers<sup>51</sup> conducted a high-throughput synthesis of a combinatorial library (>450) of homopolymers, random and block copolymers, and PEG- or other polymer-functionalized polymers. However, only nine of these variants exhibited the desired compactness and flexibility similar to bovine serum albumin.

It is worth noting that most of the above approaches focused on sophisticated designs with the considerations of intrinsic factors from the precursor itself. On the contrary, another promising approach involves manipulating the solvent conditions, which is extrinsic, to facilitate the precollapse of the precursor chains before cross-linking, mimicking the so-called hydrophobic collapse model<sup>52–54</sup> for protein folding. In this context, we achieved the compact collapse of poly(*N*-isopropylacrylamide)-based precursors via a lower critical solution temperature (LCST)-assisted coil-globule transition

in aqueous solution.<sup>6</sup> In addition, molecular dynamics simulations demonstrated that this precollapse process could also be easily achieved via a coil-globule transition induced by a cononsolvency effect.<sup>55</sup> Another important way to achieve this target is to tune the solvent quality using a mixture of poor and good solvents.<sup>28,33,56,57</sup> For instance, Satoh and co-workers<sup>28</sup> found that by doing so, the resultant SCNPs were found to be more compact than in a single good solvent condition. Such a strategy was also proven to be efficient by Diesendruck<sup>58</sup> later on for the synthesis of poly[(PMMA)-*co*-AEMA]-based SCNPs in five different solvents. More recently, the Yang group<sup>4</sup> demonstrated that adding 25% ether, a poor solvent, to the polymer solution before electrostatic-mediated intrachain cross-linking can further reduce the size of the obtained SCNPs. However, their results demonstrate that adding 50% ether leads to interchain cross-linking. Similarly, Sumerlin<sup>59</sup> found that adding a poor solvent into a good solvent can accelerate and enhance the degree of collapse of SCNPs. However, the collapsed structure of these SCNPs still deviates considerably from the native state of the protein globules. Lo Verso and co-workers<sup>60</sup> proposed the preparation of globular SCNPs in a poor solvent; however, experimentally achieving this in a purely poor solvent is challenging due to chain aggregations. Their simulations addressed this challenge by adsorbing the precursors onto a substrate surface.

Herein, we demonstrated a facile synthesis of protein-like SCNPs with compact collapse using only a low content of photoreactive cross-linking agents in a single-component poor solvent environment. In particular, polystyrene (PS) chains decorated with the photo-cross-linker 4-acryloyloxybenzophenone (ABP) were cross-linked in acetone, a typical poor solvent for PS,<sup>61,62</sup> under UV irradiation in custom-made flow chemistry equipment. The resulting SCNPs exhibited an ideal compact protein-like globular configuration (Scheme 1). In this design, the cross-linker ABP played two crucial roles: (1) It facilitated the dissolution of the PS-based precursor in acetone, enabling the chain backbone to precollapse into a globule stabilized by solvophilic ABP groups exposed on its surface. (2) Upon UV radiation, the exposed ABP units were

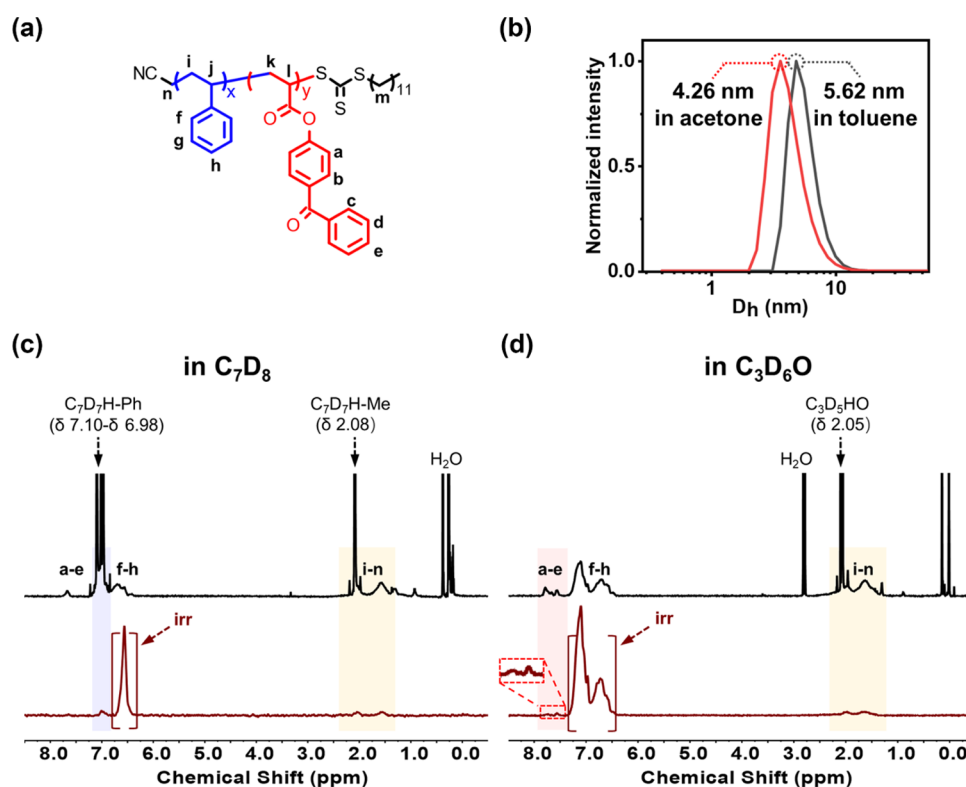


**Figure 1.** (a) Molecular structure and  $^1\text{H}$  NMR assignments of the precursors. (b) Hydrodynamic diameter ( $D_h$ ) of the precursors in acetone/toluene as determined using DLS. (c, d)  $^1\text{H}$  NMR (600 MHz) spectra (top) and NOE spectra (bottom) of precursors in  $\text{C}_7\text{D}_8$  and  $\text{C}_3\text{D}_6\text{O}$ , respectively.

excited and underwent photochemical reactions on the globule surface, effectively locking up the SCNP conformation. To unravel the underlying mechanism, we performed coarse-grained molecular dynamics (CGMD) simulations. The results demonstrate that this mechanism promotes cross-linking reactions at long contour distances along the precursor chain backbone, preserving the globular state of the SCNPs when transferred into a good solvent. Our design featured a novel approach whereby the affinity between ABP and acetone leads to exposure of the cross-linkers on the SCNP surfaces, ultimately forming reactive SCNP globules decorated with residual ABP units. This approach opens new possibilities for developing functional nanomaterials with precisely controlled folding patterns, while the inherent reactivity of SCNPs holds promise for further polymerization into hierarchical multifunctional self-assembly and diverse applications.

## RESULTS AND DISCUSSION

**Synthesis of the Precursors.** A set of linear precursors (Figure 1a) were synthesized through reversible addition–fragmentation chain transfer (RAFT) copolymerization of styrene and ABP units using 2,2′-azobis(2-methylpropanitrile) as the initiator and cyanomethyl dodecyl trithiocarbonate as the chain transfer agent. The formation of precursors was confirmed using  $^1\text{H}$  NMR and gel permeation chromatography (GPC) (Table 1 and Figures S1–S6). They were labeled as PS-ABP-Y, where Y denotes the mole fraction of ABP in the precursor chains, which were systematically varied. In the following text, the results are mainly presented for the PS-ABP-5.7 system, while others are for comparison.

**Characterization of the Solvent Environment.** To measure the solvophilicity of the precursors in different

**Table 1. Overview of the Composition (mol %), Number-Averaged Molecular Weight ( $M_n$ ), Degree of Polymerization (DP), and Molar Mass Dispersity ( $\mathcal{D}$ ) of the Precursor Chains**

sample	composition <sup>a</sup> (mol %)		$M_n^b$ (kg mol <sup>-1</sup> )	$\mathcal{D}^b$	DP <sup>c</sup>
	styrene	ABP			
PS-ABP-1.6	98.4	1.6	20.3	1.20	190
PS-ABP-2.2	97.8	2.2	21.4	1.18	199
PS-ABP-3.2	96.8	3.2	23.8	1.21	219
PS-ABP-4.3	95.7	4.3	23.0	1.26	208
PS-ABP-5.7	94.3	5.7	25.2	1.17	224
PS-ABP-24.4	75.6	24.4	29.7	1.18	211

<sup>a</sup>Calculated from  $^1\text{H}$  NMR spectra. <sup>b</sup>Determined using GPC in THF, calibrated with polystyrene standard. <sup>c</sup>Calculated from  $M_n$ .

solvents, the second osmotic virial coefficient ( $A_2$ ) was measured by using static light scattering and Zimm analysis. Positive  $A_2$  values represent an attractive force between solute and solvent molecules, corresponding to a swollen state of the precursor chain. Conversely, negative values show repulsive forces, implying a reduced state of the precursors. Here, the results for the system PS-ABP-5.7 are demonstrated, for example, as shown in Figure S7. In toluene, the  $A_2$  value was found to be  $9.418 \times 10^{-7} \text{ mol dm}^3/\text{g}^2$ , while it was  $-4.014 \times 10^{-7} \text{ mol dm}^3/\text{g}^2$  in acetone, indicating the poor solvent nature of acetone and the precollapsed state of the precursors.

To further characterize the chain conformations in both solvents, dynamic light scattering (DLS) and nuclear Overhauser effect (NOE) difference spectroscopy were performed for PS-ABP-5.7 in acetone and toluene for comparison.

**Table 2.** Overview of the Precursor PS-ABP-5.7 and the Corresponding SCNPs Synthesized at Different Exposure Times in Acetone/Toluene during Flow Chemistry<sup>a</sup>

exposure time (min)	acetone					toluene			
	$M_n^b$ (kg mol <sup>-1</sup> )	$M_w^b$ (kg mol <sup>-1</sup> )	$\bar{D}^b$	$D_h^c$ (nm)	$D^d$ ( $\times 10^{-10}$ m <sup>2</sup> s <sup>-1</sup> )	$M_n^b$ (kg mol <sup>-1</sup> )	$M_w^b$ (kg mol <sup>-1</sup> )	$\bar{D}^b$	$D_h^c$ (nm)
0 <sup>e</sup>	25.2	29.5	1.17	5.6	2.10				
8	23.8	28.8	1.21	5.0	2.22	24.1	28.2	1.16	6.9
15	21.5	26.5	1.24	4.6	2.32	21.5	27.3	1.27	4.9
30	18.2	23.4	1.29	4.3	2.57	24.0	33.1	1.38	5.7
60	12.6	18.2	1.45	3.5	2.66	23.5	41.1	1.75	6.3
90	9.2	13.3	1.44	3.3	2.90	24.7	40.4	1.64	7.0
120	8.6	12.9	1.49	3.2	2.96	24.1	42.7	1.77	7.0
10 h (in batch) <sup>f</sup>	16.2	21.4	1.33	3.9					

<sup>a</sup>The last row includes the SCNP synthesized in batch (in acetone) for 10 h, provided for comparison. <sup>b</sup>Number-averaged molecular weight  $M_n$ , weight-averaged molecular weight  $M_w$ , and polydispersity index  $\bar{D}$  are calculated from GPC in THF, calibrated with PS as standard. <sup>c</sup>Determined using DLS in chloroform at 1 mg/mL. <sup>d</sup>Diffusion coefficient  $D$  determined using DOSY measurement. <sup>e</sup>Refers to the precursor PS-ABP-5.7. <sup>f</sup>Refers to the SCNP obtained after 10 h of UV radiation in the batch system.

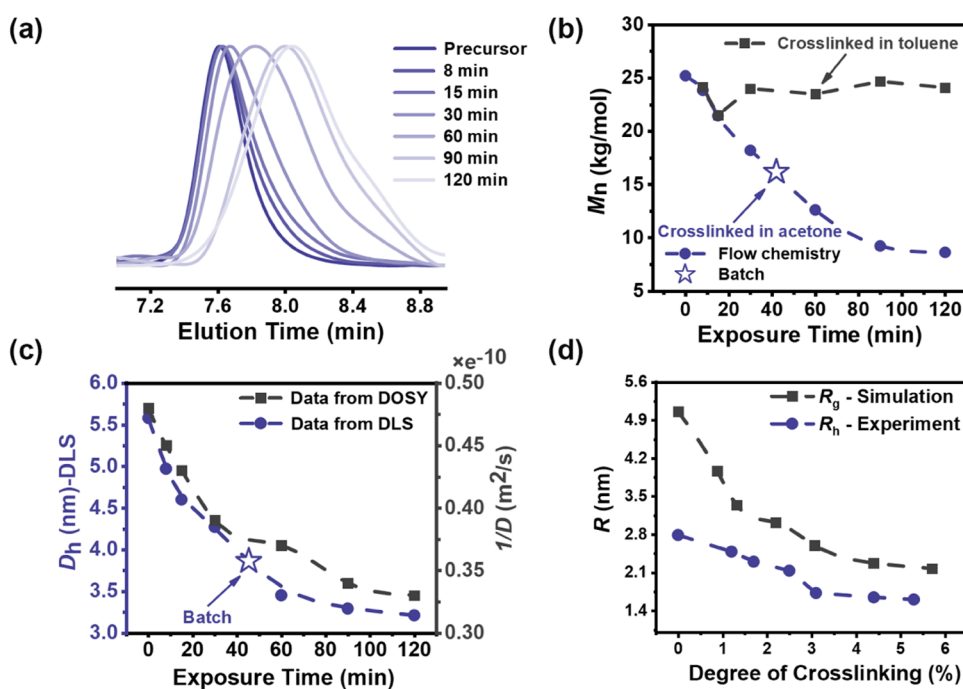


**Figure 2.** (a) GPC traces for the precursor PS-ABP-5.7 and its corresponding SCNPs synthesized in acetone at different exposure times, including 8, 15, 30, 60, 90, and 120 min. (b) Trends of the  $M_n$  of PS-ABP-5.7 cross-linked in toluene and acetone with exposure time. (c)  $D_h$  value (the left axis) from the DLS (in  $\text{CHCl}_3$ ) measurement of PS-ABP-5.7 versus exposure time, and the  $1/D$  value (the right axis) from the DOSY test (in  $\text{CDCl}_3$ ) of PS-ABP-5.7 versus exposure time. (d)  $R_h$  (from the experiment of DLS) and  $R_g$  (from CGMD simulation) of the precursor and SCNPs (cross-linked in a poor solvent) dissolved in a good solvent versus the degree of cross-linking.

Toluene was selected as the good solvent (compatible with both PS and ABP), whereas acetone was selected as the poor solvent (compatible with ABP). The DLS results (Figure 1b) demonstrate that the precursor chains exhibited a smaller hydrodynamic diameter ( $D_h$ ) in acetone compared to toluene. The 1D selective NOE results are plotted in Figure 1c,d for both solvents, alongside <sup>1</sup>H NMR spectra (which are also plotted for reference). In Figure 1c, we plot the results in deuterated toluene (a good solvent for the PS backbone of the precursor); selective irradiation of the protons on phenyl groups f–h (the right peak at ~6.60 ppm) resulted in weak signals only from the connecting backbone –CH<sub>2</sub>– (shadowed in yellow, i–n) and other protons belonging to the same phenyl groups (highlighted in purple). In contrast, we plot, in Figure 1d, the results in deuterated acetone (a poor solvent for the PS backbone of the precursor); selective irradiation of the

f–h protons resulted in response peaks from not only backbone –CH<sub>2</sub>– but also ABP (labeled as a–e; Figure 1d), indicating that the precursor chains are in a compact and collapsed state. 2D-NOESY measurements show the same trend, as supplied in Supporting Information Figures S8 and S9.

**Collapse Behavior of SCNPs in Flow Chemistry.** To achieve fine control over the intramolecular cross-linking and collapsed state of the SCNPs, SCNPs were synthesized in custom-made flow chemistry equipment with a high-pressure pump (Sanotac China) and a Philips UVA lamp (365 nm, 10 W), as illustrated in Figure S10. Flow chemistry has been revealed to exhibit higher optical and cross-linking efficiencies compared to batch methods.<sup>7</sup> Such improved efficiency allowed us to finely regulate the degree of collapse by adjusting the exposure time to UV light. In the synthesis

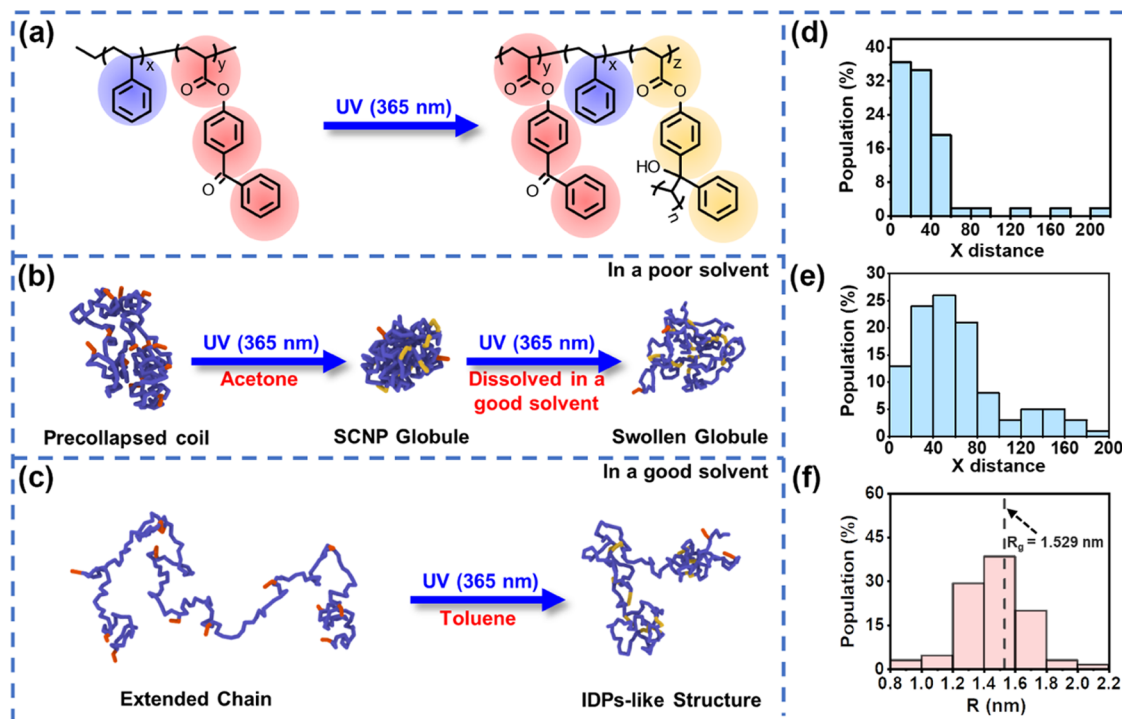


**Figure 3.** Molecular dynamics simulations for the collapse behavior of precursors. (a) Coarse-graining scheme used in our simulation. (b) SCNPs cross-linked in a poor solvent. (c) SCNPs cross-linked in a good solvent. The blue, yellow, and red beads represent the PS backbone, cross-linked ABP, and residual ABP units, respectively. Each styrene monomer is represented by one CG bead and the ABP group by three CG beads, as depicted in panel (a). The population of cross-linking reactions at different cross-linking ( $X$ ) distances along the contour in good/poor solvent were counted in panels (d) and (e), respectively. (f) Distribution of the distance of the reactive ABP units to the center of mass of the SCNPs synthesized in a poor solvent.

process, all of the precursor solutions were dissolved in acetone and pumped through a high-pressure pump into a Teflon spiral tube (inner diameter = 4.35 mm) wrapped around a UV lamp (365 nm). The exposure time was adjusted by controlling the flow rate of the precursor solutions. In particular, reactions with various exposure times were conducted: 8, 15, 30, 60, 90, and 120 min, corresponding to six different flow rates of 12.15, 6.48, 3.24, 1.62, 1.08, and 0.81 mL/min, respectively. Table 2 lists key measurements for the synthesized SCNPs resulting from cross-linking reactions of the precursor PS-ABP-5.7, including their molecular weight measured from GPC,  $D_h$  from DLS, and diffusion coefficient ( $D$ ) from diffusion-ordered spectroscopy (DOSY). Values for SCNPs synthesized through a batch photochemistry system over 10 h are also listed in the last row for comparison.

Figure 2a shows the GPC traces for precursor PS-ABP-5.7 and its corresponding SCNPs synthesized in acetone at different exposure times. As the exposure time increases, the GPC traces exhibit an apparent right shift toward longer retention time, indicating a gradual reduction in molecular size and an increase in the collapse degree of the resulting SCNPs. Figure 2b shows an exponential decay in the number-averaged molecular weight ( $M_n$ ). As the exposure time extends to 120 min, the  $M_n$  converges to a low plateau value, representing only ~34% of the precursor PS-ABP-5.7. This substantial decrease in  $M_n$  indicates a protein-like compact–collapsed behavior. In contrast, the cross-linking behavior in toluene differs completely from that in acetone. In toluene, a slight decrease in  $M_n$  is observed (Figure 2b), and both the weight-averaged molecular weight ( $M_w$ ) and the  $D_h$  value from DLS (Figure S11) are larger than that of the precursor, increasing over the

irradiation time (Table 2), indicating substantial interchain cross-linking. For comparison, the SCNPs synthesized by batch photochemistry irradiated in acetone for 10 h under UV light are represented by a star in Figure 2b. Notably, reaching a similar degree of collapse in the flow chemistry only takes ~42 min, significantly shorter than the batch process. Figure 2c provides a similar comparison for the  $D_h$  measured from DLS. Its value gradually decreases with the extension of the irradiation time, and the inverse value of  $D$  ( $1/D$ ) obtained from DOSY measurements follows a similar decreasing trend. In Figure 2d,  $R_h$  values from DLS measurement are plotted versus the real cross-linking degree (Figure S12, Tables S1 and S2) estimated from NMR spectra.

**Coarse-Grained Molecular Dynamics Simulations.** To further investigate the collapse process on the molecular scale, CGMD simulations were performed. The coarse-grain (CG) scheme, depicted in Figure 3a, represents each styrene monomer with one CG bead and each benzophenone group with three CG beads. For comparison, we simulated the collapse/cross-linking process of the precursor in both poor and good solvent conditions. Representative snapshots before and after the cross-linking in both solvent conditions are shown in Figure 3b,c, respectively (simulation details can be found in the Methods Section). As expected, SCNPs synthesized in acetone adopt compactly collapsed globule structures (Figure 3b) decorated with unreacted residual ABP groups (red) on the SCNP surface. Importantly, after post-dissolving such SCNPs in a good solvent, the globule state is maintained (the last snapshot in Figure 3b). In Figure 2d, we plot the variation of the radius of gyration ( $R_g$ ) of these SCNPs at different cross-linking degrees, post-dissolved in a good

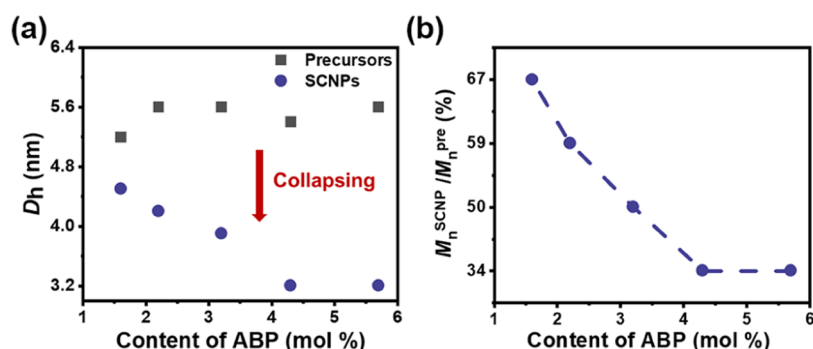


**Figure 4.** High lock-up efficiency of SCNP globules with low ABP content. (a)  $D_h$  of precursors and their corresponding SCNPs. (b) Apparent molecular weight ratio between the SCNP and the precursor  $M_n^{\text{SCNP}}/M_n^{\text{pre}}$  as a function of the content of ABP unit.

solvent. The results have a reasonable agreement of  $R_h$  values from the DLS measurement. Although DLS measurements give the value of  $R_h$  while simulations give the value of  $R_g$ , they have a reasonable size ratio of  $R_h/R_g \approx 1.7$  according to Zimm theory, and it turns out to be  $\sim 1.3$ , which is very close to the case of 3- or 4-arm star polymers.<sup>63</sup> Comparatively, our simulations demonstrate that SCNPs synthesized in a good solvent condition exhibit an IDP-like loose structure (Figure 3c). In Figure 3d,3e, we plot the distribution of the cross-linking distances ( $\Delta = i - j$ ) between cross-linked monomers  $i$  and  $j$  along the chain contour for both good and poor solvent conditions, respectively. In a good solvent (Figure 3d), cross-linking reactions mostly occur between monomer pairs with short-contour distance on the chain backbone, as these monomer pairs are physically close to each other when solvated in a good solvent. In contrast, for the intrachain reactions in a poor solvent (Figure 3e), since the precursor chains are precollapsed, cross-linking reactions are distributed over larger  $\Delta$ , effectively avoiding short-contour distance cross-linking for self-avoiding conformations in a good solvent. In Figure 3f, we plot the distance distribution of all ABP units to the center of mass of the SCNPs synthesized in a poor solvent. The results show clearly that most ABP units are distributed on the surface area of the SCNP, with the vertical dashed line indicating the  $R_g$  of SCNPs. In addition, simulations with 4 particles in a box of  $80 \sigma \times 80 \sigma \times 80 \sigma$  were performed for a long time, and no clear aggregation of particles was observed, indicating a good solubility of the particle. A snapshot of the simulation can be found in Figure S13.

**High Lock-Up Efficiency of SCNP Globules with Low ABP Content.** To further prove that SCNP-5.7-120 min has reached the collapse limit, we increased the ABP content in a precursor to 24.4% in our experiment. The variation in size of the SCNPs synthesized in this system is shown in Figure S14, with corresponding data reported in Table S3. We observed that SCNPs obtained have a similar size and degree of collapse as in the system of PS-ABP-5.7. Increasing the amount of cross-linker by  $\sim 4$  fold did not result in a further improvement of the degree of collapse. Meanwhile, to explore the minimum content of the ABP unit for an effective lock-up of the globule, we also systematically reduced the content of ABP at the fixed UV exposure time of 120 min. In Figure 4, the  $D_h$  of the precursor series and their corresponding SCNPs, along with the apparent molecular weight ratio between SCNP and the precursor ( $M_n^{\text{SCNP}}/M_n^{\text{pre}}$ ), are plotted against the ABP (cross-linker) content. Detailed data are listed in Table 3. The results indicate that a smaller content of the cross-linking agents, 4.3 mol %, can also result in a similar collapse as PS-ABP-5.7. In

**Table 3.** Hydrodynamic Diameter ( $D_h^{\text{pre}}$ ) and Number-Averaged Molecular Weight of the Precursors ( $M_n^{\text{pre}}$ ), along with the Resulting Sizes of the Corresponding SCNPs ( $D_h^{\text{SCNP}}$ ;  $M_n^{\text{SCNP}}$ ), and Their Ratios of Number-Averaged Molecular Weight ( $M_n^{\text{SCNP}}/M_n^{\text{pre}}$ ) at Various Content of ABP Unit

content of ABP (mol %)	$D_h^{\text{pre}}$ (nm)	$D_h^{\text{SCNP}}$ (nm)	$M_n^{\text{pre}}$ ( $\text{kg mol}^{-1}$ )	$M_n^{\text{SCNP}}$ ( $\text{kg mol}^{-1}$ )	$M_n^{\text{SCNP}}/M_n^{\text{pre}}$
1.6	5.2	4.5	20.3	13.5	67%
2.2	5.6	4.2	21.4	12.6	59%
3.2	5.6	3.9	23.8	11.9	50%
4.3	5.4	3.2	23.0	7.9	34%
5.7	5.6	3.2	25.2	8.6	34%
24.4 <sup>a</sup>	6.0	3.6	29.7	9.2 <sup>a</sup>	31%

<sup>a</sup>The cross-linking result of PS-ABP-24.4 was exposed by flow photochemistry at 90 min.

addition, although the degree of collapse decreases along with a further decrease in the ABP content, a very low ABP content of 1.6% can already result in an obvious collapse. The  $D_h$  data indicated a decrease of size from 5.2 to 4.5 nm. There is also a significant decrease by a molecular weight ratio of  $M_n^{\text{SCNP}}/M_n^{\text{pre}} = 67\%$ . As a strong contrast, in order to reach a similar reduction in molecular weight or hydrodynamic diameter, much higher content of cross-linker (usually 10–30 mol %) is needed in conventional approaches in good solvent.<sup>35,46</sup>

**Morphologies of the SCNP Globules.** The data above show that upon subjecting the PS-ABP precursor to photoflow chemistry in the poor solvent acetone, the resulting SCNPs obtained upon a UV exposure of 120 min exhibit the lowest apparent molecular weight, the smallest size, and consequently, the most compact structure. To visually characterize the SCNP morphology, high-resolution microscopy techniques, such as transmission electron microscopy (TEM) and atomic force microscopy (AFM), are employed. Figure 5a,5b show TEM and AFM tapping mode images, respectively, of SCNP-5.7-120 min synthesized in acetone. Both images reveal SCNPs with an average size of  $\sim 3.0$  nm. The variation in the SCNP size is reasonably consistent for both microscopy approaches, providing a reliable assessment of the SCNP globule structures.

**Determination of Form Factor from SAXS.** Small-angle X-ray scattering is an effective technique for probing the shape and structure of materials. Herein, SAXS was used to investigate the collapse state of the SCNPs during the cross-linking process. Specifically, we selected PS-ABP-5.7, SCNP-5.7-15, SCNP-5.7-60, and SCNP-5.7-120 min for SAXS analysis (Figure 6a). By analysis of the slopes of the scattering

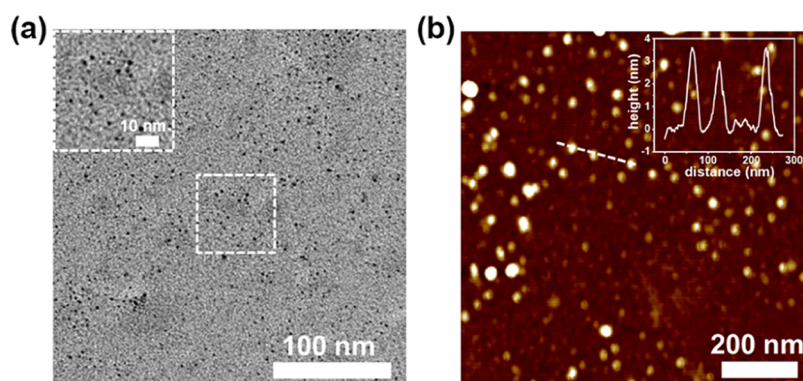


**Figure 5.** (a) TEM image of dispersed SCNP-5.7-120 min cast from the acetone solution (0.01 mg/mL). (b) AFM image of SCNP-5.7-120 min by spin-coating (0.01 mg/mL) onto a silicon surface.

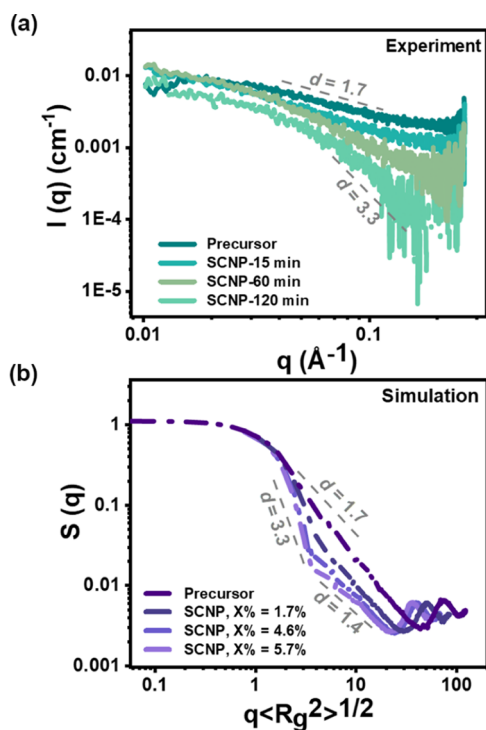


**Figure 6.** (a) SAXS scattering curves for toluene solutions at 5 mg/mL of the precursor PS-ABP-5.7, SCNP-5.7-15, SCNP-5.7-60, and SCNP-5.7-120 min synthesized in acetone solutions. (b) Calculated structure factor from simulations for SCNPs with different cross-linking degrees.

curves in the Porod regime, the fractal exponent ( $d$ ) of the polymer chain was determined as  $I \propto q^{-d}$ . The precursor PS-ABP-5.7 exhibited a curve with a slope of  $d = 1.7$ , indicating an extended self-avoiding chain conformation with a Flory exponent of  $\nu = 1/d = 0.59$ . As the UV exposure time increased, the scattering curve for the SCNPs irradiated for extended durations showed substantially pronounced slopes. For instance, the SAXS curve in the Porod regime for SCNP-5.7-120 min had a slope of close to 3.3, corresponding to a globular compact collapse with  $\nu = 1/d = 1/3$ . The slopes for other SCNPs changed smoothly between  $d = 1.7$  and 3.3, indicating a smooth transition from an extended self-avoiding chain conformation to a compact globule. Our CGMD simulations also confirmed the same trend, as shown in Figure 6b, where the calculated structure factors for SCNPs with

different cross-linking degrees are shown. Interestingly, there is a transition region in the simulation results for all SCNPs after the first fractal region, where the fractal exponent is around 1.4, which is much smaller than 1.7 and indicates stretched conformation of internal network strands between cross-linking points in the SCNPs, solvated in a good solvent.

**Reactive Self-Assembly of SCNPs.** As discussed above, the resulting SCNPs contain residual reactive ABP units and their amount varies with the UV exposure time. Therefore, we can expect these SCNPs to fabricate diverse self-assembly structures in solution. Herein, SCNP-5.7-90 min fabricated in acetone was used for further self-assembly. A 1 mg/mL tetrahydrofuran (THF) solution of SCNP-5.7-90 min was prepared and exposed to additional UV irradiation, leading to intriguing self-assembled structures in different stages. Initially, the particles were sized at  $\sim 3$  nm (Figure 7a). After  $\sim 15$  min of UV irradiation, larger particles with roughly uniform sizes around 10 nm were formed (Figure 7b). Continuing the UV irradiation for another 7 min led to the development of elongated structures with an average length of 20 nm (Figure 7c). Moreover, further irradiation for 30 min produced elongated worm-like short rods measuring 100 nm in length (Figure 7d). These findings highlight the pivotal role of residual ABP in facilitating re-cross-linking between SCNPs and driving the formation of these unique self-assembled structures. Ongoing research in our group delves into more complex reactive self-assembly processes and associated underlying mechanisms between various SCNPs.

## CONCLUSIONS

Herein, mimicking the so-called hydrophobic collapse model for protein folding, we introduced a facile strategy to fabricate protein-like compact SCNP globules. Unlike conventional approaches that start from extended self-avoiding chain conformations in a good solvent, we initiate the fabrication with precollapsed conformations of PS-based precursors in single-component poor solvent conditions. This design incorporates a small quantity of photoreactive agents (ABP) copolymerized into the precursor backbone. These ABP units act as a cross-linker and a solvophilic agent, enabling the proper dissolution of the precollapsed precursor in poor solvent conditions. Interestingly, the auxiliary solubilization effect of ABP causes the cross-linkers to be exposed to the surfaces of the PS-based polymer backbone, which differs from conventional cross-linking-driven collapsed processes, where the cross-linkers are generally evenly distributed in the interior

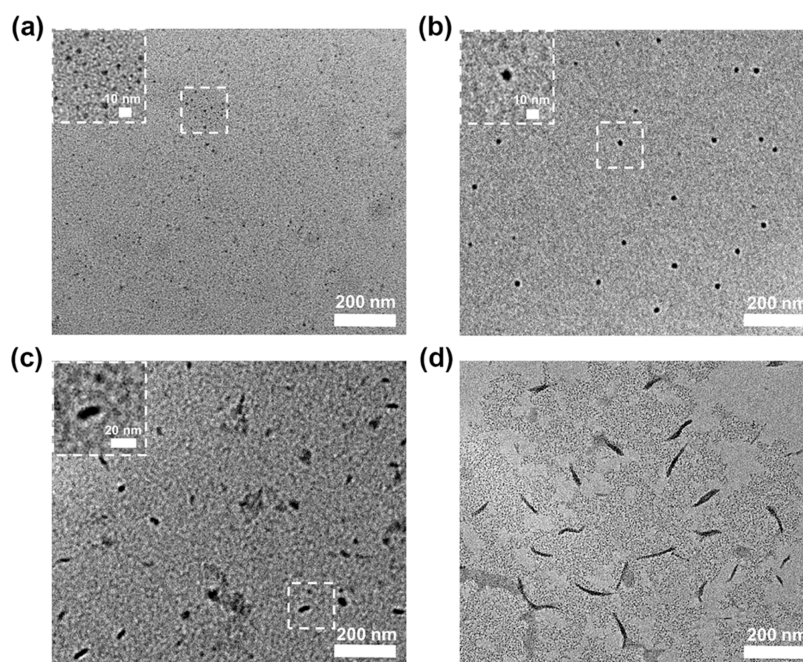


**Figure 7.** Self-assembly of reactive controllable SCNP-5.7-90 min under UV radiation. (a) Initial size of SCNP-5.7-90 min at  $\sim 3$  nm. (b–d) After exposure to UV irradiation for 15, 22, and 30 min.

of locally compact IDP domains. The cross-linking process is carried out using custom-made flow chemistry equipment, which enhances the cross-linking efficiency compared to a batch reaction. By varying the irradiation time, the internal cross-linking degree, thus the morphology of the SCNPs, can be precisely controlled. SAXS measurements show that SCNPs fabricated through this flow photochemistry-assisted process easily adopt a protein-like compactly collapsed globule structure in  $\sim 2$  h. Unexpectedly, a low cross-linking unit content of  $\sim 1.6$  mol % in this system can already result in an obvious reduction ( $M_n^{\text{SCNP}}/M_n^{\text{pre}} = 67\%$ ) in apparent molecular size, for which a much higher content of cross-linker, for instance, 10–30 mol %, was usually needed in conventionally synthesis approaches. A small content of  $\sim 4$  mol % can result in a protein-like compact collapse with  $M_n^{\text{SCNP}}/M_n^{\text{pre}} = 34\%$ . To unravel the underlying mechanism, molecular dynamics simulations were performed, indicating that the cross-linking reactions mainly occurred between ABP/monomer pairs with long contour distances along the precursor chain backbone. This inhibits the short-contour distance cross-linking reactions on extended self-avoiding chain conformations in good solvent conditions. In addition, the simulated structure factor curves align well with experimental SAXS curves. Overall, selecting a suitable solvent environment, which is a poor solvent for the precursor backbone but a good solvent for the cross-linkers, is the key to successfully fabricating SCNPs with protein-like globule structures. Our results imply the crucial role of the solvent condition in protein folding. Importantly, the UV exposure of residual reactive ABP units on the SCNP globule surface enables further utilization of the resulting SCNPs for reactive self-assembly processes, forming hierarchical multifunctional self-assembly structures. Ongoing research explores the self-assembly process, other possible structures, and associated functionalities of these SCNPs.

## METHODS

**Synthesis of Precursors.** The precursors (named PS-ABP-Y, where Y denotes the mole fraction of ABP in the precursor chains) are synthesized with styrene and ABP units through reversible addition–fragmentation chain transfer (RAFT) copolymerization using 2,2′-azobis(2-methylpropionitrile) as the initiator and cyanomethyl dodecyl trithiocarbonate as the chain transfer agent.

**Exemplary Experimental Procedure for the Synthesis of Precursor PS-ABP-5.7.** Styrene (9.9 g, 95 mmol), ABP (1.26 g, 5 mmol), cyanomethyl dodecyl trithiocarbonate (79.4 mg, 0.25 mmol), and 2,2′-azobis(2-methylpropionitrile) (AIBN) (8.2 mg, 0.05 mmol) were dissolved in anhydrous 1,4-dioxane (5 mL) in a 50 mL Schlenk tube. The mixed solution was degassed by three rigorous freeze–pump cycles in the Schlenk tube and stirred for 24 h at 363 K. Then, the Schlenk tube was cooled and ventilated to atmosphere to burst the reaction. The polymer solution was diluted by 5 mL of tetrahydrofuran (THF) and purified via precipitation in methanol. Then, the PS-ABP-5.7 was obtained by filtration as a yellow powder. The other precursors are synthesized by different feed ratios of monomers.

**Synthesis of SCNPs. Exemplary Experimental Procedure for the Synthesis of SCNPs through Photoflow Chemistry.** SCNPs were synthesized in custom-made photoflow chemistry equipment with a high-pressure pump (Sanotac China) and a Philips UVA (365 nm, 10 W) lamp, as illustrated in Figure S8. All of the precursor solutions were dissolved in acetone/toluene (0.3 mg/mL) and pumped through a high-pressure pump into a Teflon spiral tube (inner diameter = 4.35 mm) wrapped around a UV lamp (365 nm). The exposure time was adjusted by controlling the flow rate of the precursor solution. In particular, reactions with various exposure times were conducted: 8, 15, 30, 60, 90, and 120 min, corresponding to six different flow rates of 12.15, 6.48, 3.24, 1.62, 1.08, and 0.81 mL/min, respectively.

**Exemplary Experimental Procedure for the Synthesis of SCNPs through a Batch System.** The precursor solutions were dissolved in acetone (0.3 mg/mL) in a 500 mL three-neck round-bottom flask with a full jacket at 25 °C. Then, the solution was irradiated with 365 nm UV light for 10 h.

After evaporation to remove acetone/toluene, SCNPs were diluted by a small amount of THF and purified via precipitation in methanol. The SCNPs were obtained by filtration as a yellow powder.

**Simulation Method and Details.** The coarse-grained mapping scheme is shown in Scheme S1, where one PS monomer is represented by one A bead (in blue) and one ABP monomer is represented by three B beads (in red). Explicit solvent S beads were used to simulate the solvent environment. All simulations were performed using HOOMD-BLUE packages. Lennard–Jones potential was used to describe the nonbonded interactions between different CG bead pairs,

$$U(r) = \begin{cases} 4\epsilon \left[ \left( \frac{\sigma}{r} \right)^{12} - \left( \frac{\sigma}{r} \right)^6 \right] & \text{for } r < r_c \\ 0 & \text{for } r \geq r_c \end{cases}$$

where  $\epsilon$  is the interaction strength between different interaction pairs,  $\sigma$  is the size of CG beads, and  $r_c$  is the cutoff of potential. Chemical bonds between CG beads in the precursor were described with harmonic potential.

**Model Parametrization.** To develop the CG model, one top-down method is applied to parametrize the potential, in which the structural property mean square radius of gyration ( $R_g$ ) is used for reference physical quantity. The  $R_g$  is calculated from simulations,

$$R_g = \sqrt{\frac{1}{N} \sum_N (R_i - R_{cm})^2}$$

where  $N$  is the number of units for a certain configuration,  $R_i$  is the coordinate of its unit, and  $R_{cm}$  is the center of mass of the configuration. First, a single precursor chain was generated by random walking in the simulated box using the in-house script, after which we added the solvent to a number density of 0.85. The chain length is set as 250, which is consistent with the experiment, and the size of the box is set to be at least twice greater than the end-to-end distance of the precursor chain to avoid the unphysical boundary effect. To build the relationship between the real and reduced units, we adopt the size of the CG bead as 0.4 nm according to hard-core size calculated from atomistic simulations of PS. Interaction strength is set as  $\epsilon_{AA} = \epsilon_{BB} = \epsilon_{SS} = 1.0 k_B T$  for interaction bead pairs with the same bead type. In order to simulate the impact of the solvent environment on the PS monomer, we carry out a sequence of simulations with varied interaction strength between A and S beads from 0.8 to 1.2  $k_B T$ . A total of 2 000 000 steps are performed for sampling configurations with a time step  $dt = 0.005\tau$ . The simulation temperature is set at  $T = 1.0 k_B T$ , which is controlled with a Nose–Hoover thermostat under an NVT ensemble with a temperature coupling constant  $\tau_T = 0.5$ . Each simulation has eight parallel runs. We found that 0.9 and 1.1  $k_B T$  corresponded well to the experimental  $R_g$  in good solvent and poor solvent environments (5.06 nm; 2.1 nm; 2.13 nm), respectively. Thus, we think that backbone monomer A (styrene) has an interaction strength of  $\epsilon_{BS} = 1.1 k_B T$  in toluene and 0.9  $k_B T$  in acetone. In order to simulate the solvophilicity of the ABP unit, B-type beads were always set to have an interaction strength with solvent of  $\epsilon_{BS} = 1.1 k_B T$ . The detailed interaction strength parameters are listed in Table 4.

**Cross-Linking Details.** Well-balanced configurations of precursors under different solvent environments are used to perform cross-linking reactions. The cross-linker is randomly distributed along the backbone. The judgment of the cross-linking reaction is as follows: (1) The distance between the ends of the two cross-linking agents must be less than 1  $\sigma$ . (2) The cross-linker site is greater than 14 PS

**Table 4. Interaction Strength  $\epsilon$  between CG Beads Used in Our Simulation<sup>64</sup>**

good/poor	A	B	S
A	1.0		
B	1.0	1.0	
S	1.1(toluene)/0.9(acetone)	1.1	1.0

monomers (about 2 Kuhn lengths) along the backbone. A total of 2 000 000 steps are performed for the cross-linking reaction, and a judgment is made every 50 000 steps. The conformations of SCNPs with different degrees of cross-linking were collected and then placed in different solvent environments for other 2 000 000-step sampling simulations. Eight parallel samples for every sampling simulation were used for ensemble averaging.

## ■ ASSOCIATED CONTENT

### Supporting Information

The Supporting Information is available free of charge at <https://pubs.acs.org/doi/10.1021/acs.macromol.3c01863>.

Materials and instrumentations; characterizations of polymers and SCNPs; and additional characterization data (PDF)

## ■ AUTHOR INFORMATION

### Corresponding Author

Hu-Jun Qian – State Key Laboratory of Supramolecular Structure and Materials, College of Chemistry, Jilin University, Changchun 130012, China; [orcid.org/0000-0001-8149-8776](https://orcid.org/0000-0001-8149-8776); Email: [hjqian@jlu.edu.cn](mailto:hjqian@jlu.edu.cn)

### Authors

Lei Zhang – State Key Laboratory of Supramolecular Structure and Materials, College of Chemistry, Jilin University, Changchun 130012, China

Xu-Ze Zhang – State Key Laboratory of Supramolecular Structure and Materials, College of Chemistry, Jilin University, Changchun 130012, China

Jia-Tong Lyu – College of Chemistry, Jilin University, Changchun 130012, China

Lin-Xiuzi Yu – State Key Laboratory of Supramolecular Structure and Materials, College of Chemistry, Jilin University, Changchun 130012, China

Chun-Yu Wang – State Key Laboratory of Supramolecular Structure and Materials, College of Chemistry, Jilin University, Changchun 130012, China

Zhao-Yan Sun – State Key Laboratory of Polymer Physics and Chemistry, Changchun Institute of Applied Chemistry, Chinese Academy of Sciences, Changchun 130022, China; [orcid.org/0000-0002-6357-3039](https://orcid.org/0000-0002-6357-3039)

Zhong-Yuan Lu – State Key Laboratory of Supramolecular Structure and Materials, College of Chemistry, Jilin University, Changchun 130012, China; [orcid.org/0000-0001-7884-0091](https://orcid.org/0000-0001-7884-0091)

Complete contact information is available at: <https://pubs.acs.org/10.1021/acs.macromol.3c01863>

### Author Contributions

H.J.Q. conceived the project and led the design in both the experiment and the simulations. L.Z. codesigned the experiment and carried out most of the experimental synthesis and characterizations. L.Z. and H.J.Q. cowrote the manuscript with input from other coauthors. X.Z.Z. and L.X.Z.Y. performed the computer simulations. C.Y.W. tested the DOSY and NOE in the experimental section. J.T.L. carried out part of the experimental synthesis and characterizations. Z.Y.S. and Z.Y.L. cosupervised the project. All authors discussed the results and commented on the manuscript.

### Notes

The authors declare no competing financial interest.

## ACKNOWLEDGMENTS

This research is supported by the National Key Research and Development Program of China (2022YFB3707302) and by the National Natural Science Foundation of China (22133002, 52293471, and 21873040). The authors acknowledge the State Key Laboratory of Supramolecular Structure and Materials and the High-Performance Computing Center of Jilin University. H.-J.Q. and Z.-Y.L. also acknowledge the support from the Program for JLU Science and Technology Innovative Research Team.

## REFERENCES

- (1) Dill, K. A.; MacCallum, J. L. The protein-folding problem, 50 years on. *Science* **2012**, *338* (6110), 1042–1046.
- (2) Archontakis, E.; Deng, L.; Zijlstra, P.; Palmans, A. R. A.; Albertazzi, L. Spectrally PAINTing a Single Chain Polymeric Nanoparticle at Super-Resolution. *J. Am. Chem. Soc.* **2022**, *144* (51), 23698–23707.
- (3) Kodura, D.; Rodrigues, L. L.; Walden, S. L.; Goldmann, A. S.; Frisch, H.; Barner-Kowollik, C. Orange-Light-Induced Photochemistry Gated by pH and Confined Environments. *J. Am. Chem. Soc.* **2022**, *144* (14), 6343–6348.
- (4) Shao, Y.; Wang, Y.-L.; Tang, Z.; Wen, Z.-D.; Chang, C.-W.; Wang, C.-Y.; Sun, D.-Y.; Ye, Y.-L.; Qiu, D.; Ke, Y.-B.; Liu, F.; Yang, Z.-Z. Scalable Synthesis of Photoluminescent Single-Chain Nanoparticles by Electrostatic-Mediated Intramolecular Crosslinking. *Angew. Chem., Int. Ed.* **2022**, *61* (27), No. e202205183.
- (5) Watanabe, K.; Kaizawa, N.; Ree, B. J.; Yamamoto, T.; Tajima, K.; Isono, T.; Satoh, T. One-Shot Intrablock Cross-Linking of Linear Diblock Copolymer to Realize Janus-Shaped Single-Chain Nanoparticles. *Angew. Chem., Int. Ed.* **2021**, *60* (33), 18122–18128.
- (6) Zhang, H.; Zhang, L.; You, J.-C.; Zhang, N.; Yu, L.; Zhao, H.-Y.; Qian, H.-J.; Lu, Z.-Y. Controlling the Chain Folding for the Synthesis of Single-Chain Polymer Nanoparticles Using Thermoresponsive Polymers. *CCS Chem.* **2021**, *3* (8), 2143–2154.
- (7) Galant, O.; Donmez, H. B.; Barner-Kowollik, C.; Diesendruck, C. E. Flow Photochemistry for Single-Chain Polymer Nanoparticle Synthesis. *Angew. Chem., Int. Ed.* **2021**, *60* (4), 2042–2046.
- (8) Xiang, D.; Chen, X.; Tang, L.; Jiang, B.-Y.; Yang, Z.-Z. Electrostatic-Mediated Intramolecular Cross-Linking Polymers in Concentrated Solutions. *CCS Chem.* **2019**, *1* (5), 407–430.
- (9) Galant, O.; Bae, S.; Silberstein, M. N.; Diesendruck, C. E. Highly Stretchable Polymers: Mechanical Properties Improvement by Balancing Intra- and Intermolecular Interactions. *Adv. Funct. Mater.* **2019**, *30* (18), No. 1901806, DOI: 10.1002/adfm.201901806.
- (10) Chen, T.; Zhao, H.-Y.; Shi, R.; Lin, W.-F.; Jia, X.-M.; Qian, H.-J.; Lu, Z.-Y.; Zhang, X.-X.; Li, Y.-K.; Sun, Z.-Y. An unexpected N-dependence in the viscosity reduction in all-polymer nanocomposite. *Nat. Commun.* **2019**, *10* (1), No. 5552.
- (11) Hosono, N.; Kushner, A. M.; Chung, J.; Palmans, A. R.; Guan, Z.; Meijer, E. W. Forced unfolding of single-chain polymeric nanoparticles. *J. Am. Chem. Soc.* **2015**, *137* (21), 6880–6888.
- (12) Chen, J.-F.; Li, K.; Shon, J. S. L.; Zimmerman, S. C. Single-Chain Nanoparticle Delivers a Partner Enzyme for Concurrent and Tandem Catalysis in Cells. *J. Am. Chem. Soc.* **2020**, *142* (10), 4565–4569.
- (13) Chen, J.-F.; Wang, J.; Bai, Y.-G.; Li, K.; Garcia, E. S.; Ferguson, A. L.; Zimmerman, S. C. Enzyme-like Click Catalysis by a Copper-Containing Single-Chain Nanoparticle. *J. Am. Chem. Soc.* **2018**, *140* (42), 13695–13702.
- (14) Liu, Y.-L.; Paulohrl, T.; Presolski, S. I.; Albertazzi, L.; Palmans, A. R.; Meijer, E. W. Modular Synthetic Platform for the Construction of Functional Single-Chain Polymeric Nanoparticles: From Aqueous Catalysis to Photosensitization. *J. Am. Chem. Soc.* **2015**, *137* (40), 13096–13105.
- (15) Terashima, T.; Mes, T.; De Greef, T. F. A.; Gillissen, M. A. J.; Besenius, P.; Palmans, A. R. A.; Meijer, E. W. Single-chain folding of polymers for catalytic systems in water. *J. Am. Chem. Soc.* **2011**, *133* (13), 4742–4745.
- (16) Rothfuss, H.; Knofel, N. D.; Roesky, P. W.; Barner-Kowollik, C. Single-Chain Nanoparticles as Catalytic Nanoreactors. *J. Am. Chem. Soc.* **2018**, *140* (18), 5875–5881.
- (17) Zeng, R.-J.; Chen, L.; Yan, Q. CO<sub>2</sub>-Folded Single-Chain Nanoparticles as Recyclable, Improved Carboxylase Mimics. *Angew. Chem., Int. Ed.* **2020**, *59* (42), 18418–18422.
- (18) Liu, Y.-L.; Pujals, S.; Stals, P. J. M.; Paulohrl, T.; Presolski, S. I.; Meijer, E. W.; Albertazzi, L.; Palmans, A. R. A. Catalytically Active Single-Chain Polymeric Nanoparticles: Exploring Their Functions in Complex Biological Media. *J. Am. Chem. Soc.* **2018**, *140* (9), 3423–3433.
- (19) Hamelmann, N. M.; Paulusse, J. M. J. Single-chain polymer nanoparticles in biomedical applications. *J. Controlled Release* **2023**, *356*, 26–42.
- (20) Kröger, A. P. P.; Paulusse, J. M. J. Single-chain polymer nanoparticles in controlled drug delivery and targeted imaging. *J. Controlled Release* **2018**, *286*, 326–347.
- (21) Liao, S.; Wei, L.; Bouchez, A. E.; Stellacci, F. Influence of structural dynamics on cell uptake investigated with single-chain polymeric nanoparticles. *Chem.* **2023**, *9* (6), 1562–1577.
- (22) Mundsinger, K.; Tuten, B. T.; Wang, L.; Neubauer, K.; Kropf, C.; O'Mara, M. L.; Barner-Kowollik, C. Visible-Light-Reactive Single-Chain Nanoparticles. *Angew. Chem., Int. Ed.* **2023**, *62* (23), No. e202302995.
- (23) Frisch, H.; Menzel, J. P.; Bloesser, F. R.; Marschner, D. E.; Mundsinger, K.; Barner-Kowollik, C. Photochemistry in Confined Environments for Single-Chain Nanoparticle Design. *J. Am. Chem. Soc.* **2018**, *140* (30), 9551–9557.
- (24) Feist, F.; Menzel, J. P.; Weil, T.; Blinco, J. P.; Barner-Kowollik, C. Visible Light-Induced Ligation via o-Quinodimethane Thioethers. *J. Am. Chem. Soc.* **2018**, *140* (37), 11848–11854.
- (25) Hoffmann, J. F.; Roos, A. H.; Schmitt, F. J.; Hinderberger, D.; Binder, W. H. Fluorescent and Water Dispersible Single-Chain Nanoparticles: Core-Shell Structured Compartmentation. *Angew. Chem., Int. Ed.* **2021**, *60* (14), 7820–7827.
- (26) Mavila, S.; Eivgi, O.; Berkovich, I.; Lemcoff, N. G. Intramolecular Cross-Linking Methodologies for the Synthesis of Polymer Nanoparticles. *Chem. Rev.* **2016**, *116* (3), 878–961.
- (27) Beck, J. B.; Killops, K. L.; Kang, T.; Sivanandan, K.; Bayles, A.; Mackay, M. E.; Wooley, K. L.; Hawker, C. J. Facile Preparation of Nanoparticles by Intramolecular Crosslinking of Isocyanate Functionalized Copolymers. *Macromolecules* **2009**, *42* (15), 5629–5635.
- (28) Watanabe, K.; Tanaka, R.; Takada, K.; Kim, M.-J.; Lee, J.-S.; Tajima, K.; Isono, T.; Satoh, T. Intramolecular olefin metathesis as a robust tool to synthesize single-chain nanoparticles in a size-controlled manner. *Polym. Chem.* **2016**, *7* (29), 4782–4792.
- (29) Moreno, A. J.; Lo Verso, F.; Sanchez-Sanchez, A.; Arbe, A.; Colmenero, J.; Pomposo, J. A. Advantages of Orthogonal Folding of Single Polymer Chains to Soft Nanoparticles. *Macromolecules* **2013**, *46* (24), 9748–9759.
- (30) Roy, R. K.; Lutz, J. F. Compartmentalization of single polymer chains by stepwise intramolecular cross-linking of sequence-controlled macromolecules. *J. Am. Chem. Soc.* **2014**, *136* (37), 12888–12891.
- (31) Fischer, T. S.; Schulze-Sunninghausen, D.; Luy, B.; Altintas, O.; Barner-Kowollik, C. Stepwise Unfolding of Single-Chain Nanoparticles by Chemically Triggered Gates. *Angew. Chem., Int. Ed.* **2016**, *55* (37), 11276–11280.
- (32) Mes, T.; van der Weegen, R.; Palmans, A. R.; Meijer, E. W. Single-chain polymeric nanoparticles by stepwise folding. *Angew. Chem., Int. Ed.* **2011**, *50* (22), 5085–5089.
- (33) Liao, S.-Y.; Wei, L.-X.; Abriata, L. A.; Stellacci, F. Control and Characterization of the Compactness of Single-Chain Nanoparticles. *Macromolecules* **2021**, *54* (24), 11459–11467.
- (34) Perez-Baena, I.; Asenjo-Sanz, I.; Arbe, A.; Moreno, A. J.; Lo Verso, F.; Colmenero, J.; Pomposo, J. A. Efficient Route to Compact Single-Chain Nanoparticles: Photoactivated Synthesis via Thiol–Yne Coupling Reaction. *Macromolecules* **2014**, *47* (23), 8270–8280.

- (35) Pomposo, J. A.; Perez-Baena, I.; Lo Verso, F.; Moreno, A. J.; Arbe, A.; Colmenero, J. How Far Are Single-Chain Polymer Nanoparticles in Solution from the Globular State? *ACS Macro Lett.* **2014**, *3* (8), 767–772.
- (36) van der Lee, R.; Buljan, M.; Lang, B.; Weatheritt, R. J.; Daughdrill, G. W.; Dunker, A. K.; Fuxreiter, M.; Gough, J.; Gsponer, J.; Jones, D. T.; Kim, P. M.; Kriwacki, R. W.; Oldfield, C. J.; Pappu, R. V.; Tompa, P.; Uversky, V. N.; Wright, P. E.; Babu, M. M. Classification of intrinsically disordered regions and proteins. *Chem. Rev.* **2014**, *114* (13), 6589–6631.
- (37) Sanchez-Sanchez, A.; Akbari, S.; Etxeberria, A.; Arbe, A.; Gasser, U.; Moreno, A. J.; Colmenero, J.; Pomposo, J. A. "Michael" Nanocarriers Mimicking Transient-Binding Disordered Proteins. *ACS Macro Lett.* **2013**, *2* (6), 491–495.
- (38) Moreno, A. J.; Lo Verso, F.; Arbe, A.; Pomposo, J. A.; Colmenero, J. Concentrated Solutions of Single-Chain Nanoparticles: A Simple Model for Intrinsically Disordered Proteins under Crowding Conditions. *J. Phys. Chem. Lett.* **2016**, *7* (5), 838–844.
- (39) Harth, E.; Horn, B. V.; Lee, V. Y.; Germack, D. S.; Gonzales, C. P.; Miller, R. D.; Hawker, C. J. A Facile Approach to Architecturally Defined Nanoparticles via Intramolecular Chain Collapse. *J. Am. Chem. Soc.* **2002**, *124*, 8653–8660.
- (40) Hanlon, A. M.; Lyon, C. K.; Berda, E. B. What Is Next in Single-Chain Nanoparticles? *Macromolecules* **2016**, *49* (1), 2–14.
- (41) Beil, J. B.; Lemcoff, N. G.; Zimmerman, S. C. On the Nature of Dendrimer Cross-Linking by Ring-Closing Metathesis. *J. Am. Chem. Soc.* **2004**, *126* (42), 13576–13577.
- (42) Kamtekar, S.; Schiffer, J. M.; Xiong, H.; Babik, J. M.; Hecht, M. H. Protein design by binary patterning of polar and nonpolar amino acids. *Science* **1993**, *262*, 1680–1685.
- (43) Anfinsen, C. B. Principles that govern the folding of protein chains. *Science* **1973**, *181*, 223–230.
- (44) Dill, K. A. Dominant forces in protein folding. *Biochemistry* **1990**, *29* (31), 7133–7155.
- (45) Anfinsen, C. B. The formation and stabilization of protein structure. *Biochem. J.* **1972**, *128* (128), 737–749.
- (46) ter Huurne, G. M.; Palmans, A. R.; Meijer, E. W. Supramolecular Single-Chain Polymeric Nanoparticles. *CCS Chem.* **2019**, 64–82, DOI: 10.31635/ccschem.019.20180036.
- (47) ter Huurne, G. M.; de Windt, L. N. J.; Liu, Y.-L.; Meijer, E. W.; Voets, I. K.; Palmans, A. R. A. Improving the Folding of Supramolecular Copolymers by Controlling the Assembly Pathway Complexity. *Macromolecules* **2017**, *50* (21), 8562–8569.
- (48) Gillissen, M. A. J.; Terashima, T.; Meijer, E. W.; Palmans, A. R. A.; Voets, I. K. Sticky Supramolecular Grafts Stretch Single Polymer Chains. *Macromolecules* **2013**, *46* (10), 4120–4125.
- (49) ter Huurne, G. M.; Voets, I. K.; Palmans, A. R. A.; Meijer, E. W. Effect of Intra- versus Intermolecular Cross-Linking on the Supramolecular Folding of a Polymer Chain. *Macromolecules* **2018**, *51* (21), 8853–8861.
- (50) Wijker, S.; Deng, L.; Eisenreich, F.; Voets, I. K.; Palmans, A. R. A. En Route to Stabilized Compact Conformations of Single-Chain Polymeric Nanoparticles in Complex Media. *Macromolecules* **2022**, *55* (14), 6220–6230.
- (51) Upadhyaya, R.; Murthy, N. S.; Hoop, C. L.; Kosuri, S.; Nanda, V.; Kohn, J.; Baum, J.; Gormley, A. J. PET-RAFT and SAXS: High Throughput Tools to Study Compactness and Flexibility of Single-Chain Polymer Nanoparticles. *Macromolecules* **2019**, *52* (21), 8295–8304.
- (52) Bhatia, S.; Udgaonkar, J. B. Heterogeneity in Protein Folding and Unfolding Reactions. *Chem. Rev.* **2022**, *122* (9), 8911–8935.
- (53) Dill, K. A. Theory for the folding and stability of globular proteins. *Biochemistry* **1985**, *24* (6), 1501–1509.
- (54) Agashe, V. R.; Shastry, M. C. R.; Udgaonkar, J. B. Initial hydrophobic collapse in the folding of barstar. *Nature* **1995**, *377*, 754–757.
- (55) Zhang, Y.-Y.; Jia, X.-M.; Shi, R.; Li, S.-J.; Zhao, H.-Y.; Qian, H.-J.; Lu, Z.-Y. Synthesis of Polymer Single-Chain Nanoparticle with High Compactness in Cosolvent Condition: A Computer Simulation Study. *Macromol. Rapid Commun.* **2020**, *41* (24), No. e1900655.
- (56) Liu, C. H.; Dugas, L. D.; Bowman, J. I.; Chidanguro, T.; Storey, R. F.; Simon, Y. C. Forcing single-chain nanoparticle collapse through hydrophobic solvent interactions in comb copolymers. *Polym. Chem.* **2020**, *11* (2), 292–297.
- (57) Basasoro, S.; Gonzalez-Burgos, M.; Moreno, A. J.; Verso, F. L.; Arbe, A.; Colmenero, J.; Pomposo, J. A. A Solvent-Based Strategy for Tuning the Internal Structure of Metallo-Folded Single-Chain Nanoparticles. *Macromol. Rapid Commun.* **2016**, *37* (13), 1060–1065.
- (58) Levy, A.; Goldstein, H.; Brenman, D.; Diesendruck, C. E. Effect of Intramolecular Crosslinker Properties on the Mechanochemical Fragmentation of Covalently Folded Polymers. *J. Polym. Sci.* **2020**, *58* (5), 692–703.
- (59) Scheutz, G. M.; Elgoyhen, J.; Bentz, K. C.; Xia, Y.-N.; Sun, H.; Zhao, J.-P.; Savin, D. A.; Sumerlin, B. S. Mediating covalent crosslinking of single-chain nanoparticles through solvophobicity in organic solvents. *Polym. Chem.* **2021**, *12* (31), 4462–4466.
- (60) Lo Verso, F.; Pomposo, J. A.; Colmenero, J.; Moreno, A. J. Simulation guided design of globular single-chain nanoparticles by tuning the solvent quality. *Soft Matter* **2015**, *11* (7), 1369–1375.
- (61) Rebelo, L. P.; Van Hook, W. A. An unusual phase diagram: The polystyrene acetone system in its hypercritical region; near tricritical behavior in a pseudo-binary solution. *J. Polym. Sci., Part B: Polym. Phys.* **1993**, *31*, 895–897, DOI: 10.1002/polb.1993.090310719.
- (62) Rebelo, L. P.; Visak, Z. P.; Szydłowski, J. Metastable critical lines in (acetone + polystyrene) solutions and the continuity of solvent-quality states. *Phys. Chem. Chem. Phys.* **2002**, *4* (6), 1046–1052.
- (63) Rubinstein, M.; Colby, R. H. *Polymer Physics*; Oxford University Press: New York, 2003; Vol. 53, pp 1394–1395 DOI: 10.1002/pi.1472.
- (64) Anderson, J. A.; Glaser, J.; Glotzer, S. C. HOOMD-blue: A Python package for high-performance molecular dynamics and hard particle Monte Carlo simulations. *Comput. Mater. Sci.* **2020**, *173*, 109363–109368.